Int. J. Electrochem. Sci., 14 **(2019)** 5738 – 5747, doi: 10.20964/2019.06.02

International Journal of
ELECTROCHEMICAL
SCIENCE
www.electrochemsci.org

Facile Fabrication of CF_x-Pt Composites as a High-Performance Cathode for Primary Lithium Batteries

LingXiao Zhang, LiJuan Zhang[*], *LiDeGe Xi*

Beijing Key Laboratory for Green Catalysis and Separation, Department of Chemistry and Chemical Engineering, School of Environmental and Energy Engineering, Beijing University of Technology
Corresponding Author: Lijuan Zhang
[*]E-mail: zhanglj1997@bjut.edu.cn

Received: 28 January 2019 / *Accepted:* 10 March 2019 / *Published:* 10 May 2019

In the present work, graphite fluoride-platinum(CF_x-Pt) composites synthesized via a novel and simple in situ method are discussed as very promising cathodes for primary lithium-ion batteries. The influence of platinum on the performance of CF_x was investigated through X-ray diffraction, X-ray photoelectron spectroscopy, transmission electron microscopy, high-resolution transmission electron microscopy and electrochemical measurements. We found that the emergence of semi-ionic C-F bonds and the uniform dispersion of platinum on the surface of CF_x during the modification process are the most important factors for improving the electrochemical performance of the cathode material. With the conductivity provided by the platinum, the CF_x-Pt cathode achieved a higher discharge capacity and a higher rate capability compared with those of the pristine CF_x cathode; the CF_x-Pt cathode exhibited a discharge capacity of 600 mAh g^{-1}, an excellent power density of 8692 W kg^{-1} at a current density of 5 C, and a plateau of 2.0 V. More importantly, as a kind of lubricant, CF_x makes it difficult to uniformly disperse modifying materials across its surface. However, our method opens a new avenue for the better dispersion of modifying materials on the surface of CF_x.

1. INTRODUCTION

Li/CF_x batteries possess the highest theoretical specific capacity (865 mAh g^{-1}) and theoretical specific energy density (2180 Wh kg^{-1}) among all commercially available primary lithium batteries, which have been influential in society.[1-4] Li/CF_x batteries have been widely explored and applied in military weapons, implantable medical devices, defense tools and aerospace devices because of their advantages of a wide operational temperature range (-40~170 ℃), high open circuit voltage (3.0~3.2 V), low self-discharge and long shelf life.[5-10] However, current Li/CF_x batteries suffer from their low operating discharge voltage and poor high-rate performance, mainly due to the kinetic limitations

associated with the poor electrical conductivity of CF_x induced by the strongly covalent C-F bond, which has inhibited the widespread commercialization of Li/CF_x batteries in modern society.[11-15]

To solve these problems, researchers have applied different approaches to improve the conductivity of CF_x in recent years. For instance, a series of carbon subfluoride materials have been reported that improved the electrochemical performance of CF_x materials.[16,17] Adding a small amount of a secondary cathode material with good conductivity, such as metal oxides, to CF_x was shown to be a very effective method to reduce or eliminate the voltage delay of CF_x.[18,19] In a recent report, Zhu et al. developed a simple and novel method for the first synthesis of SiO_2-modified CF_x, and CF_x-mSiO_2 could achieve a discharge capacity of 587 mAh g^{-1} with a plateau of 2.28 V at a current density of 5 C.[20] Zhong et al. prepared fluorinated multilayered graphene (GF_x) by direct gas fluorination of RGO instead of graphene oxide. The cathode delivered a high energy density of 1073 Wh kg^{-1} and an excellent power density of 21460 W kg^{-1} at a high current density of 10 A g^{-1}.[21] Other methods have included the enhancement of the conductivity of CF_x by the coating of a conductive material onto the surface of CF_x, such as carbon and polyaniline.[22,23] It has been proven that these methods are effective for improving the rate performance of Li/CF_x batteries. Platinum (Pt)-based materials are generally considered to be the most effective electrocatalysts for the HER because of their advantages of a high activity, a high selectivity and environmental friendliness.[24,25] To date, numerous researchers have realized the dispersion of Pt-based catalysts as either single atoms or subnanometer clusters on supports and have obtained good electrochemical performance. However, current reports on improving the conductivity of cathode material by Pt-modified CF_x are comparatively scarce in primary lithium-ion batteries. In this paper, we utilize the improved conductivity of a metal platinum-modified CF_x cathode material, and the as-synthesized CF_x-Pt material displays a discharge capacity of 600 mAh g^{-1} with a plateau of 2.0 V at a current density of 5 C.

In this work, we successfully synthesized CF_x-supported Pt clusters through a novel and simple method to load noble metals onto CF_x in situ. The platinum nanoparticles produced by this method could be more effectively distributed than by previous methods. The structures, morphologies and electrochemical performance of all samples were investigated. The results indicate that the CF_x-Pt materials exhibit excellent electrochemical properties, especially high rate performance.

2. EXPERIMENTAL PROCEDURE

2.1. Synthesis of the samples

The CF_x-Pt composites were fabricated as follows. First, CF_x powders (Hubei, Graphite precursor, $x \geq 0.8$) was dispersed in 30 mL of water and ethanol at 80 ℃ with rigorous stirring for 30 min in a water bath. Then, a 0.01 M aqueous $H_2PtCl_6 \cdot 6H_2O$ solution was added to the suspension, and the mixture was stirred at 353 K for 3 h. Then, the resulting precipitate was washed with a mixed water/ethanol solution several times and freeze-dried overnight. The final CF_x-Pt was obtained by annealing the above product at 623 K for 3 h in air.

2.2. Material Characterization

X-ray diffraction (XRD) was performed using a Bruker D8 Advance diffractometer with Cu Kα radiation (λ=0.15406 nm). Transmission electron microscopy (TEM) and high-resolution transmission electron microscopy (HRTEM) images were obtained using a Tecnai F20 microscope in conjunction with powder samples deposited onto a copper microgrid. XPS spectra were acquired using a Kratos AxisUltra XPS spectrometer with an Al Kα X-ray source and an energy resolution of 0.48 eV.

2.3. Electrochemical measurements

For the electrochemical tests, the cathode materials (80% by weight), PVDF resin (10% by weight) and acetylene black (10% by weight) were mixed and stirred evenly in N-methyl-2-pyrrolidone (NMP) to form a uniform black slurry. The mixture was coated onto aluminum foil current collectors and then dried in a vacuum oven at 80 ℃ for 6 h. Then, the electrode was cut into disks 14 mm in diameter, and the disks were dried at 120 ℃ for 24 h. Finally, the disks were transferred into a dry glovebox filled with argon for cell assembly. The CR2032-type coin cells were assembled with a metallic lithium disc as the anode, a microporous polypropylene as the separator, and 1 mol L^{-1} $LiPF_6$ (EC–DMC, 1:1 *w/w*) as the electrolyte. The coin cells were discharged on a NEWARE battery test station with a cut-off voltage of 1.5 V and were discharged at different rates at room temperature. Electrochemical impedance spectroscopy (EIS) measurements were carried out on an electrochemical workstation (VMP3, Biopic Logic SA) over a frequency range from 100 kHz to 10 MHz.

3. RESULTS AND DISCUSSION

XRD was used to analyze the compositions of the prepared materials, as shown in Fig. 1. From the XRD patterns, all samples had three typical wide peaks at 2θ values of 13.4°, 25.7° and 41.2°, which indicated that the structure of the pristine CF_x was not changed during modification with Pt. The peaks at 2θ=13.4° correspond to the (001) plane of CF_x, especially for the compounds with high fluorine content.[26] The peaks at 2θ=25.7° could be assigned to the (002) plane of graphite.[27-29] The peaks at 2θ=41.2° were attributed to the (100) plane of graphite, which is related to the C-C in-plane length.[30-32] Moreover, diffraction peaks at 2θ values of 39.8°, 46.3° and 67.5° were observed in the XRD patterns of CF_x-Pt corresponding to the (111), (200) and (220) planes, respectively, of the face-centered cubic structure of the platinum nanoparticles (JCPDS 04-0802, a=3.923 α=90°).[33-35] The diffraction peaks of fcc Pt at 2θ=39.8°, 46.3° and 67.5° were broad, indicating a high dispersion and a smaller size for the Pt nanoparticles. A typical XPS survey scan and the surface composition of the samples are shown in Fig. 1b. The XPS survey spectra of both CF_x and CF_x-Pt display C 1s, O 1s, N 1s and F 1s peaks, corroborating the presence of carbon, oxygen, nitrogen and fluorine. In addition, the CF_x-Pt materials display a predominant peak at 72 eV corresponding to Pt 4f, confirming the presence of platinum.

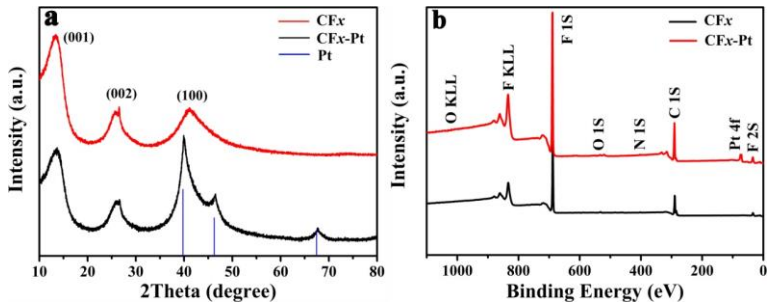

Figure 1. (a) XRD patterns of CF_x and CF_x-Pt and (b) the full XPS spectra of CF_x and CF_x-Pt

The morphologies of the samples were studied using transmission electron microscopy (TEM). Fig. 2(a-c) show the TEM images of the platinum nanoparticles, which are uniformly dispersed across the surface and edges of the layered CF_x support. The rough surface of CF_x might expose a greater number of active sites during modification with the Pt NPs, which would improve the interaction of the Pt NPs and result in a uniform dispersion of the platinum nanoparticles without aggregation. The analysis of the elemental distribution of the samples was performed using energy dispersive X-ray spectrometry (EDS) mapping. Fig. 2d shows the uniform distribution of the C, F, and Pt elements in the sample corresponding to the broadening of the Pt peaks in the XRD pattern. Fig. 2(e-h) show high-resolution TEM (HRTEM) images of the CF_x-Pt material, and the HRTEM images clearly show characteristic lattice spacings of 0.226 nm and 0.196 nm, which are consistent with the (111) and (200) lattice planes of Pt.[36,37] The Pt (111) and Pt (200) facets were clearly observed, indicating the close contact between the Pt NPs and supporting CF_x, which is favorable for charge transfer at these interfaces.

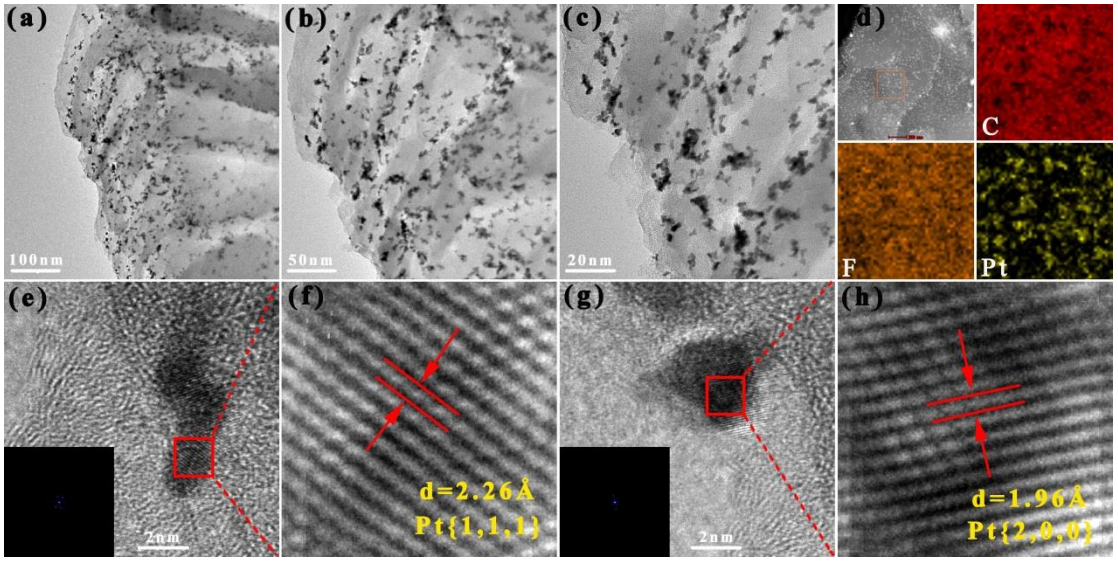

Figure 2. (a-c) TEM images of CF_x-Pt, (d) HAADF-STEM-EDS mapping of CF_x-Pt and (e-h) HRSTEM images of CF_x-Pt.

To analyze the chemical states and elemental compositions of all samples, X-ray photoelectron spectroscopy (XPS) analysis was carried out. The corresponding results are shown in Fig. 3a-d. Fig. 3a

and 3b show the XPS spectra of both CF_x and CF_x-Pt, and there were five peaks in the C 1s region. The peak located at 284.8 eV corresponded to sp^2 C=C bonding, and that located at 286.3 eV was assigned to sp^3 C-C bonding.[38,39] The additional peaks at approximately 288.0 eV, 290.3 eV and 291.5 eV corresponded to semi-ionic C-F, covalent C-F and C-F_2 bonding, respectively.[38,40-42] As shown in Fig. 3c, the peaks located at 71.4 eV and 75.0 eV corresponded to Pt $4f_{7/2}$ and Pt $4f_{5/2}$, respectively, indicating the normal Pt° state in the CF_x-Pt materials,[43] which is consistent with the XRD results. Fig. 3d shows the F 1s spectra of both CF_x and CF_x-Pt. It can be seen that the peak for CF_x-Pt shows a small shift compared with that of pristine CF_x, which is due to covalent C-F bonds transforming into semi-ionic C-F bonds. Furthermore, the presence of semi-ionic C-F was beneficial for improving the conductivity of the material.[44]

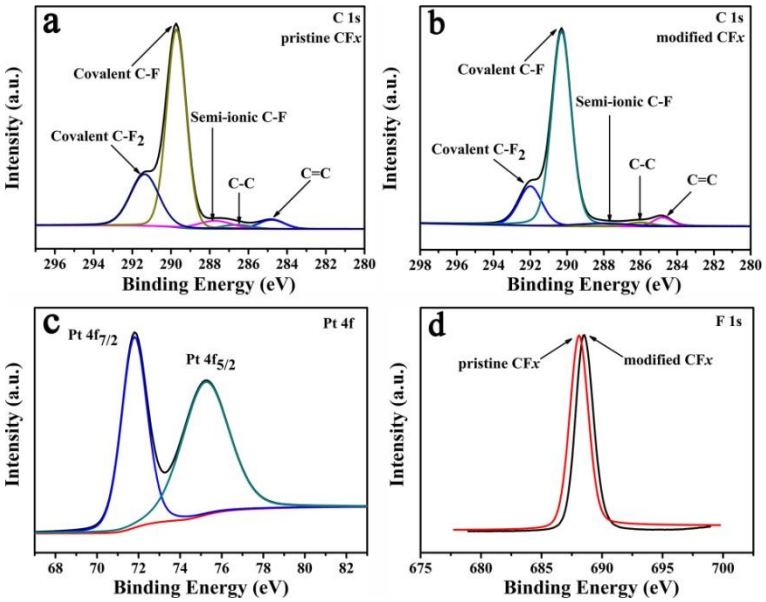

Figure 3. High-resolution XPS spectra of CF_x and CF_x-Pt: (a and b) C 1s, (c) Pt 4f and (d) F 1s.

CR2032-type cells with a metallic Li counter electrode were used to investigate the electrochemical performance of the pristine CF_x and CF_x-Pt composites at different current rates (Fig. 4), and the electrochemical performance of the pristine CF_x and CF_x-Pt composites are listed in Table 1. As shown in Fig. 4(a-b), at rates of 0.05 C, 0.5 C, 1 C, 2 C and 5 C, the discharge capacities of pristine CF_x were 665, 611, 603, 495 and 217 mAh g^{-1},respectively, while for CF_x-Pt, the discharge capacities were 848, 729, 691, 681 and 600 mAh g^{-1}, respectively. Although an optimal conducting agent (10% acetylene black) was used, the pristine CF_x still showed a poor discharge specific capacity at different current rates compared with those of the CF_x-Pt composite. More interestingly, whereas CF_x cathodes are known to suffer from slow kinetics, the CF_x-Pt electrodes demonstrated outstanding high rate capabilities. The specific capacities of the pristine CF_x cathodes at the rates of 2 C and 5 C were 495 and 217 mAh g^{-1}, respectively. Compared with those of pristine CF_x, the CF_x-Pt samples exhibited higher discharge capacities of 681 and 600 mAh g^{-1} at 2 C and 5 C, respectively, with a significant increase in the specific capacity. Even at a rate of 5 C, only a marginal change was observed in the

discharge capacity. In summary, the electrochemical properties of the CF_x cathode materials prepared in this paper exhibited better properties than those of most of the currently available CF_x cathodes. For instance, carbon fluoride (CF_x)/manganese dioxide (MnO_2) hybrid cathodes display a maximum power density of only 6599 W kg^{-1} and an energy density of only 1814 Wh kg^{-1} at 5 C.[19] This is mainly because these hybrid materials could only improve the discharge performance of the battery to a certain extent because the CF_x materials and MnO_2 materials cannot be integrally combined by simple mechanical milling. PPy-CF_x composite materials were synthesized by electrodeposition, and they exhibited a discharge capacity of only 70 mAh g^{-1} at 4 C.[45] Carbon subfluoride nanofibers (F:C=0.76) can achieve a high power density of 8057 W kg^{-1} at 6 C.[46] However, the discharge capacity of the carbon subfluoride nanofibers substantially decreased at high rates. Fig. 4c shows the average potentials of the pristine CF_x and CF_x-Pt composites as a function of the discharge rate. At rates of 0.05 C, 0.5 C, 1 C, 2 C and 5 C, the average discharge voltages of pristine CF_x were 2.4, 2.2, 2.1, 1.8 and 1.7 V, respectively, while for CF_x-Pt, the average discharge voltages were 2.4, 2.3, 2.2, 2.1 and 2.0 V, respectively. Obviously, the average potential of the pristine CF_x rapidly decreased with an increasing discharge rate, and its average potential was only 1.7 V at a discharge rate of 5 C. In comparison to pristine CF_x, the CF_x-Pt samples exhibited a higher discharge voltage of 2 V at 5 C. Fig. 4d shows the energy density versus power density (Ragone plots) of all samples, and higher energy density and the lower power density values were observed at low discharge rates. With an increasing discharge rate, the energy density obviously decreased due to a drop in the output potential and discharge capacity.

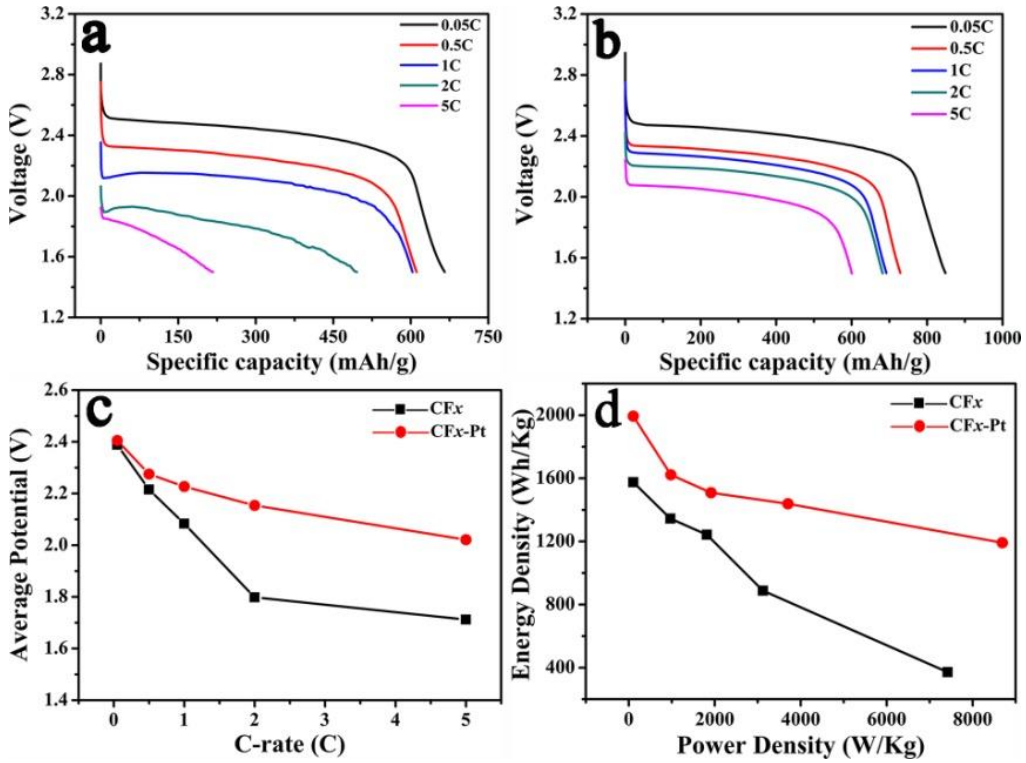

Figure 4. The galvanostatic discharge curves of (a) CF_x and (b) CF_x-Pt, (c) the average potential as a function of the discharge rate and (d) the Ragone plot of the pristine CF_x and CF_x-Pt composite.

Table 1. Electrochemical performances of both cells.

Samples	C-rate	Average Potential (E/V)	Specific Capacity (mAh/g)	Energy density (Wh/Kg)	Average Power Density(W/kg)
CF_x	0.05C	2.4	665	1575	104
	0.5 C	2.2	611	1345	967
	1 C	2.1	603	1242	1816
	2 C	1.8	495	888	3121
	5 C	1.7	217	372	7418
CF_x-Pt	0.05C	2.4	848	1994	104
	0.5 C	2.3	729	1622	978
	1 C	2.2	691	1509	1915
	2 C	2.1	681	1439	3705
	5 C	2.0	600	1192	8692

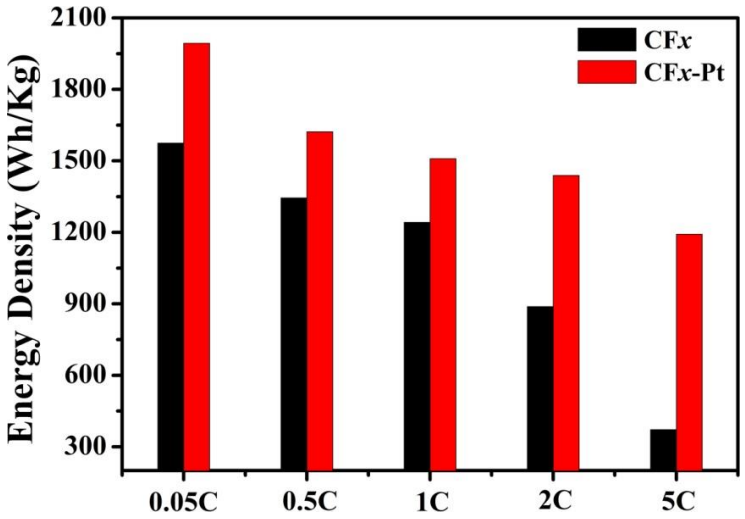

Figure 5. Gravimetric energy densities of the CF_x samples at different current densities

However, the energy density was almost three times greater for CF_x-Pt at a rate of 5 C compared with that of the pristine CF_x (Fig. 5). At the same time, the Ragone plot indicates that the CF_x-Pt exhibited the best performance among all samples. For a high rate, the CF_x-Pt composite power density was more than 8692 W kg^{-1} (at a 5 C discharge rate), whereas a power density of only 7418 W kg^{-1} was obtained for the pristine CF_x.

The electronic conductivity of the electrode material, the diffusion of lithium within the electrode and the integrity of the electrode-electrolyte interface could be further researched by electrochemical impedance spectroscopy (EIS). Fig. 6 shows the Nyquist plots of the battery cells prepared with CF_x-Pt and pristine CF_x in their discharged states. All samples had a sloped straight line in the low-frequency region and a semicircle in the high-frequency region, which represent the Li^+ transfer resistance between the electrolyte and the surface of the electrode and the charge-transfer

resistance at the interface of the electrode and electrolyte, respectively. As shown in Fig. 6, the charge transfer impedance of the pristine CF_x cathode was approximately 195 Ω, which is approximately 4 times greater than that of the CF_x-Pt cathode (44 kΩ). It was obvious that the impedance could be reduced through Pt modification of the cathode, resulting in a higher discharge capacity and discharge platform. The EIS measurement provides further evidence for the improvement of the electrochemical performance through the introduction of metallic Pt.

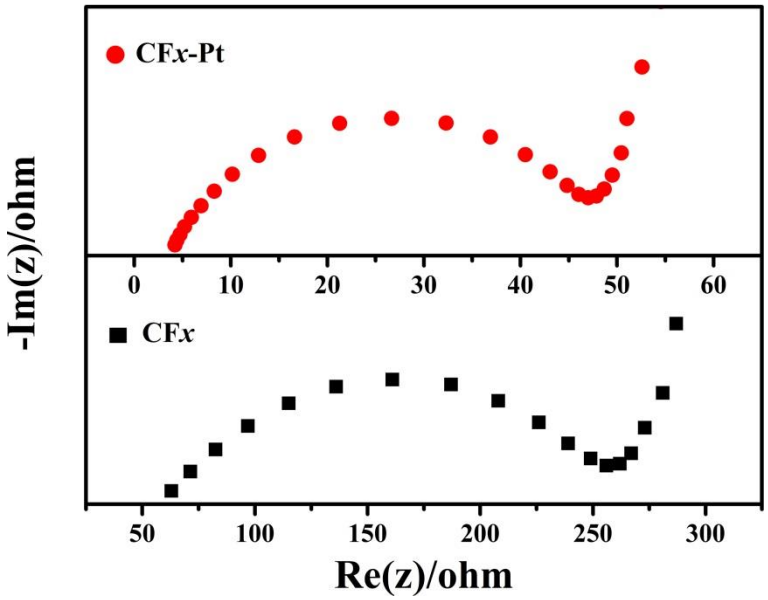

Figure 6. Impedance spectra of CF_x and CF_x-Pt

4. CONCLUSION

In summary, we have synthesized CF_x-Pt materials by a simple in situ chemical modification method, and small platinum nanoparticles are uniformly dispersed across the CF_x surface. The phases and chemical structures of the CF_x-Pt materials were characterized by X-ray diffraction and X-ray photoelectron spectroscopy. The surface morphology and elemental mapping were studied using transmission electron microscopy and high-resolution transmission electron microscopy. Interestingly, the CF_x-Pt materials show a discharge capacity of 600 mAh g^{-1} with a plateau of 2.0 V and a maximum power density of 8692 W kg^{-1} at a current density of 5 C. The CF_x-Pt materials show better electrochemical properties compared to those of pristine CF_x, which may be due to the emergence of semi-ionic C-F bonds and the decrease in the charge transfer resistance after the platinum nanoparticles have been uniformly dispersed across the CF_x materials during the modification process.

ACKNOWLEDGMENTS
This work was supported by Beijing municipal high level innovative team building program, Beijing University of Technology (IDHT20180504), The National Natural Science Foundation of China (51472009) and 17 Connotation Development-Curriculum and Teaching Material Construction-Quality Teaching Resources Project, Beijing University of Technology (310000514117026).

References

1. L. Li, L. Zhu, Y. Pan, W.X. Lei, Z.S. Ma, Z.Z. Li, J.J. Cheng and J. Zhou, *Int. J. Electrochem. Sci.*, 11 (2016) 6838-6847.
2. P.J. Sideris, R. Yew, I. Nieves, K. Chen, G. Jain, C.L. Schmidt and S.G. Greenbaum, *J. Power Sources*, 254 (2014) 293-297.
3. L. Zhu, L. Li, J. Zhou, Y. Pan, W.X. Lei and Z.S. Ma, *Int. J. Electrochem. Sci.*, 11 (2016) 6413-6422.
4. D. Damien, P.M. Sudeep, T.N. Narayanan, M.R. Anantharaman, P.M. Ajayan and M.M. Shaijumon, *RSC Adv.*, 3 (2013) 25702-25706.
5. J. Lee, A. Urban, X. Li, D. Su, G. Hautier and G Ceder, *Science*, 343 (2014) 519-522.
6. A.G. Ritchie, C.O. Giwa, P.G. Bowles, J. Burgess, E. Eweka and A. Gilmour, *J. Power Sources*, 96 (2001) 180-183.
7. J. Liu, H. Xia, D. Xue and L. Lu, *J. Am. Chem. Soc.*, 131 (2009) 12086-12087.
8. T. Nakajima, *J. Fluorine Chem.*, 149 (2013) 104-111.
9. G. Nagasubramanian, *Int. J. Electrochem. Sci.*, 2 (2007) 913-922.
10. J.C. Lu, Z.C. Liu, P. Huang, Q. Fang and M.H. Zhu, *Advanced Materials Research*, 704 (2013) 98-101.
11. E.Z. Kurmaev, A. Moewes, D.L. Ederer, H. Ishii, K. Seki and M. Yanagihara, *Phys. Lett. A*, 288 (2001) 340-344.
12. P. Meduri, H. Chen, X. Chen, J. Xiao, M.E. Gross and T.J. Carlson, *Electrochem. Commun.*, 13 (2011) 1344-1348.
13. H. Groult, C.M. Julien, A. Bahloul, S. Leclerc, E. Briot and A. Mauger, *Electrochem. Commun.*, 13 (2011) 1074-1076.
14. M. Dubois, K. Guérin, W. Zhang, Y. Ahmad, A. Hamwi and Z. Fawal, *Electrochim. Acta*, 59 (2012) 485-491.
15. K. Guérin, M. Dubois, A. Houdayer and H. André, *J. Fluorine Chem.*, 134 (2012) 11-17.
16. R. Yazami, A. Hamwi, K. Guérin, Y. Ozawa, M. Dubois and J. Giraudet, *Electrochem. Commun.,* 9 (2007) 1850-1855.
17. J. Giraudet, C. Delabarre, K. Guérin, M. Dubois and F. Masin, *J. Power Sources*, 158 (2006) 1365-1372.
18. M. Nagata, J. Yi and M. Tomcsi, *ECS Trans.*, 33 (2011) 223-237.
19. Y. Li and W. Feng, *J. Power Sources*, 274 (2015) 1292-1299.
20. Y.L. Zhu, L.J. Zhang, H.H. Zhao and Y. Fu, *J Mater Chem A*, 5 (2017) 796-803.
21. G. Zhong, H. Chen, X. Huang, H. Yue and C. Lu, *Frontiers in chemistry*, 6 (2018) 50.
22. L. Zhu, Y. Pan and L. Li, *Int. J. Electrochem. Sci.*, 11 (2016) 14-22.
23. E. Frackowiak and K. Jurewicz, *Adv. Mater. Opt. Electron.*, 8 (1998) 303-308.
24. S.A. Grigoriev, P. Millet and V.N. Fateev, *J. Power Sources*, 177 (2008) 281-285.
25. M.C. Tavares, S.A.S. Machado and L.H. Mazo, *Electrochim. Acta*, 46 (2002) 4359-4369.
26. K. Guérin, J.P. Pinheiro, M. Dubois, Z. Fawal, F. Masin, R. Yazami and A. Hamwi, *Chem. Mater.*, 16 (2004) 1786-1792.
27. A. Hamwi, *J. Phys. Chem. Solids*, 57 (1996) 677-688.
28. Z. Wang, J. Wang, Z. Li, P. Gong, J. Ren and H. Wang, *RSC Adv.*, 2 (2012) 11681-11686.
29. C. Nethravathi and M. Rajamathi, *Carbon*, 46 (2008) 1994-1998.
30. P. Meduri, H. Chen, J. Xiao, J.J. Martinez, T. Carlson and J.G. Zhang, *J Mater Chem A*, 1 (2013) 7866.
31. S. Mouras, A. Hamwi, D. Djurado and J.C. Cousseins, *Cheminform*, 24 (1988) 572.
32. P. Gong, Z. Wang, J. Wang, H. Wang, Z. Li and Z. Fan, *J Mater Chem*, 22 (2012) 16950.
33. L. Hyosun, L. Juhyung, L. Changhwan, B. Seoin, A. Kwangjin and S.J. Won, *Nat. Commun.*, 9 (2018）2235.

34. Y.C. Hsieh, Y. Zhang, D. Su, V. Volkov, R. Si and L. Wu, *Nat Commun*, 4 (2013) 2466.
35. X.X. Wang, Z.H. Tan, M. Zeng and J.N. Wang, *Surf. Sci. Rep.*, 4 (2014) 4437.
36. D.B. Gorle and M.A. Kulandainathan, *J Mater Chem A*, 5 (2017) 15273-15286.
37. Y. Li, M. Mao, Q. Zhang, Y. Yang, H. Huang and Z. Jiang, *Green Chem.*, 20 (2018) 2857-2869.
38. X. Guangran, S. Rui, L. Jiayin, Z. Luyao, G. Xia and G. Rui, *J Mater Chem A*, 6 (2018) 12759-12767.
39. M. Ren, X. Wang, C. Dong, B. Li, Y. Liu and T. Chen, *Phys. Chem. Chem. Phys.*, 17 (2015) 24056-24062.
40. P.F. Fulvio, S.S. Brown, J. Adcock, R.T. Mayes, B. Guo and X.G. Sun, *Chem. Mater.*, 23 (2015) 4420-4427.
41. P. Gong, Z. Wang, Z. Li, Y. Mi, J. Sun and L. Niu, *Rsc Adv.*, 3 (2013) 6327-6330.
42. S. Yan, J. Zhao, Y. Yuan, S. Liu, Z. Huang and Z. Chen, *Rsc Adv.*, 3 (2013) 21869-21876.
43. S.A. Abbas, S.H. Kim, M.I. Iqbal, S. Muhammad, W.S. Yoon and K.D. Jung, *Sci. Rep.*, 8 (2018) 2986.
44. P. Chandran, A. Ghosh and S. Ramaprabhu, *Sci Rep*. 8 (2018) 3591.
45 H. Groult, C. Julien, A. Bahloul, S. Leclerc, E. Briot and A. Mauger, *Electrochem. Commun*. 13 (10) (2011) 1074-1076.
46 R. Yazami, A. Hamwi, K. Guérin, Y. Ozawa, M. Dubois, J. Giraudet and F. Masin, *Electrochem. Commun.*, 9 (2007) 1850.